A low carbon route to ethylene: Ethane oxidative dehydrogenation with CO2 on embryonic zeolite supported Mo-carbide catalyst

Vera Bikbaeva, Nikolay Nesterenko, Stanislav Konnov, Thanh-Son Nguyen, Jean-Pierre Gilson, Valentin Valtchev

A Low Carbon Route to Ethylene: Ethane Oxidative Dehydrogenation with CO_2 on Embryonic Zeolite Supported Mo-Carbide Catalyst

Vera Bikbaeva,[a] Nikolay Nesterenko,[b,*,≠] Stanislav Konnov,[a] Thanh-Son Nguyen,[b] Jean-Pierre Gilson,[a] Valentin Valtchev[a]

Affiliations

[a] Laboratoire Catalyse et Spectrochimie, ENSICAEN, Université de Caen, CNRS, 6 Boulevard Maréchal Juin, 14050 Caen, France
[b] TotalEnergies One Tech Belgium, Zone Industrielle C, 7181 Seneffe, Belgium

Highlights

- Embryonic zeolite supported Mo_2C catalyst is prepared and comprehensively characterized
- The catalyst is employed for oxidative dehydrogenation of ethane with CO_2 (ODH-CO_2)
- The proposed catalyst allows designing a potentially CO_2 negative technology
- 109% of CO_2 reduction in comparison to state-of-the-art ethane cracker is achieved
- A techno-economical analysis of the proposed ODH-CO_2 process is performed

Abstract

The study reports a novel catalyst based on supported molybdenum-carbide (Mo_2C) phase for oxidative dehydrogenation of ethane with CO_2 (ODH-CO_2). The optimal result is obtained with MoS_2-precursor as the intermediate supported on a non-acidic embryonic zeolite, which is transformed *in situ* to Mo_2C (Mo_2C@EZ). The ultimate catalyst and its intermediates are characterized. 66 % conversion of ethane, 58 % of ethylene yield, and 56% conversion of CO_2 to CO with the *in situ* co-produced hydrogen obtained from ethane to ethylene transformation are the achievements of utilizing Mo_2C@EZ. The performed techno-economic study on Mo_2C@EZ results in a potentially CO_2 negative route for ethylene production with 109% of CO_2 reduction per ton of produced ethylene in comparison with a conventional ethane cracker. The process is expected to be cheaper in capital expenditure (CAPEX) and operating expenses (OPEX) thanks to a simpler product slate, lower energy demand, and no requirement for steam dilution.

[≠] Corresponding author current address: Sulzer, Neuwiesenstrasse 15, 8401 Winterthur, Switzerland; E-mail: nikolay.nesterenko@sulzer.com

Keywords

CO_2 utilization; Oxidative dehydrogenation; Embryonic zeolite; Mo modification, CO_2 negative ethylene production

1. Introduction

Ethylene is the largest-volume petrochemical building block, produced primarily by steam cracking of oil fractions [1]. In 2020, the worldwide ethylene production capacity was 201 million tons, with an expected increase to 263 million tons in 2030 [2,3]. Ethylene is used to produce a wide spectrum of products like plastics, fibers, and other chemicals in the packaging, transportation, and construction industries. Polyethylene is the single-largest outlet, accounting for about 60% of global ethylene consumption in 2020. Other major applications include the production of ethylene oxide, ethylene dichloride, and ethylbenzene.

Steam cracking of oil fractions is the major process currently used to produce ethylene; a smaller contribution comes from refinery processes such as fluid catalytic crackers and cokers. It is a mature and well-established technology, which operation is considered near-optimal considering constant incremental improvements of the technology over 80^{+} years [4,5], leading to a thermal efficiency of close to 95% [6]. However, cracking is a very endothermic reaction taking place at high temperatures. As a result, ethylene production via steam cracking consumes about 30 % of the energy used in the chemical industry. In particular, as ethylene production by steam cracking consumes roughly between 17-25 GT/ton of ethylene while releasing about 1.2 tons of CO_2 per ton of olefin produced [5]; it is with about 260 million tons of CO_2 emissions worldwide per year [6], one of the largest contributors to greenhouse gas emissions in the manufacturing sector. Alternative routes and feedstocks need to be explored and developed to foster sustainable development of olefins production. In the last decade, the ongoing shift to lighter hydrocarbons as steam cracking feedstock has prompted research and development of alternative on-purpose production routes to ethylene.

One of the options for sustainable ethylene production is in the utilization of bio feedstock: either bioethanol or bio hydrocarbon fractions [7–9]. Bioethanol dehydration shows advantages in energy consumption and in capital investments relative to conventional steam cracking due to simpler product slate and lower reaction temperature. Until the mid-1940s, a significant portion of the ethylene produced industrially was produced from bioethanol. Afterward, steam cracking of hydrocarbons, because of their superior economies of scale and lower feedstock costs, became the main source of ethylene. Currently, with the significantly increased cost of natural gas and crude oil together with the need to reduce the carbon intensity of the petrochemical industry, the downstream industry is renewed interest in ethylene-from-ethanol plants [10,11]. So, this route will certainly regain importance but will not fulfill the total

demand for ethylene due to the competition for the feedstock with biofuel production. The availability of bio-naphtha and bio-propane as a feedstock for olefins production is still limited [8]. The direct conversion of the cellulosic biomass or bio-oil remains an attractive route but mainly provides aromatic fractions [12–14].

So, a reduction of the carbon intensity of ethylene production routes remains a very important task for the petrochemical industry. The oxidative dehydrogenation of ethane (ODH) shows good prospects to reduce greenhouse gases emissions in comparison to a conventional ethane cracker due to a number of advantages, including lower energy consumption, simpler production slate, and potential elimination of the equilibrium limitations [15,16]. One of the main limitations remains the development of an efficient and stable high-temperature catalyst. Already in the early 80's, Phillips Petroleum proposed the first industrial Li-$SnCl_2$-MgO catalyst for oxidative dehydrogenation of ethane with oxygen [17]. This process did not require acetylene hydrogenation and had the potential to reduce energy consumption in an ethylene plant, allowing operations at 700 °C instead of 850 °C, and providing a higher ultimate yield of 90.5% ethylene [17] compared to the thermal process. However, as CO_2 was an important by-product, the economics were not better than state-of-the-art steam crackers. Recently, the topic regain attention the two semi-commercial oxidative dehydrogenation (ODH) of ethane processes were proposed [18–20]. Oxygen as an oxidant could be used in gaseous form or from catalysts' metal oxides lattice. One such promising on-purpose Oxidative Dehydrogenation of Ethane (ODH-E) technology is proposed by the Linde/Clariant partnership; a high selectivity to valuable products (ethylene and acetic acid) compared to steam cracking combined with a significant reduction potential of the CO_2 footprint is promised. Moreover, the reaction takes place under mild conditions, for instance, at atmospheric pressure and a maximum temperature of 400 °C [21]. However, as oxygen is applied as an oxidant, CO_2 is still present in products.

Another ODH option is based on chemical looping (CL-ODH). In CL-ODH, ethane is oxidatively dehydrogenated to ethylene and water following a typical Mars-van Krevelen mechanism with the participation of lattice oxygen from the catalyst (Catalyst reduction, Reaction 1a) and its exothermic air regeneration (Reaction 1b), further providing heat to the endothermic ethane dehydrogenation to ethylene [22].

CL-ODH (Reduction)

$$C_2H_6 + Me_yO_x \rightarrow C_2H_4 + H_2O + Me_yO_{x-1}$$ (Reaction 1a)

CL-ODH (Regeneration)

$$Me_yO_{x-1} + 1/2O_2 \rightarrow Me_yO_x$$ (Reaction 1b)

Other alternative approaches, currently at the laboratory scale, also using CO_2 as an oxidant to produce value-added ethylene from ethane, are proposed [18,19]. Such processes are attractive because they may lead to a CO_2-negative route in ethylene production. An additional benefit is a significant decrease in energy consumption downstream as hydrogen will not need purification: it will be consumed *in situ* to convert CO_2 to CO, and the latter could further be used to produce methanol, carbonylate, or hydroformylate other feedstocks. This approach is particularly interesting in view of recent trends to "electrify" steam crackers [23–25].

It is of note that the enthalpies of reactions 2 and 3 ($\Delta_rH^o_{298}$) to produce ethylene from ethane by steam cracking and ODH-CO_2 are very close:

$$C_2H_6(g) + CO_2(g) \rightarrow C_2H_4(g) + CO(g) + H_2O\ (l), \quad \Delta_rH^o_{298} = 134\ kJ/mol\ (Reaction\ 2)$$

$$C_2H_6(g) \rightarrow C_2H_4(g) + H_2(g)\ (2), \quad \Delta_rH^o_{298} = 137\ kJ/mol\ (Reaction\ 3)$$

The ODH-CO_2 reaction was first reported by Lunsford *et al*. [26] using Li/MgO catalysts. Krylov *et al*. [27] investigated the ODH-CO_2 using several oxide catalysts (Fe_2O_3, Cr_2O_3, MnO_2) and multi-component systems. In the ODH-CO_2 at 800 °C, MnO_2-based catalysts exhibited high activities but low ethylene selectivity [28]. Nakagawa *et al*. [29] studied the dehydrogenation of C_2H_6 by CO_2 on several oxides and reported that gallium oxide (Ga_2O_3) is an effective catalyst for this reaction, giving a C_2H_4 yield of 18.6% with a selectivity of 94.5% at 650 °C.

Several reactions may occur in parallel, including oxidative dehydrogenation (ODH), reverse water-gas-shift (RWGS), or dry reforming of ethane (DRE) [30]. For the ODH-CO_2 reaction, precious metals, oxide [31], and carbide [30]-based catalysts are reported. Most of the catalytic systems are based on Pt [32], Ni [33], Co [34], Cr [35,36], Fe [37] oxides deposited on zeolite or oxide carriers.

Only a few Mo-based materials were reported for the ODH-CO_2 of ethane [38–40], but molybdenum carbide is well known as an alternative catalyst to noble metals in the highly selective reduction of CO_2 to CO [41,42]. Very high conversions of ethane in co-processing with CO_2 to produce hydrogen, ethylene, and CO were reported on the catalysts made up of the oxides of cobalt and molybdenum [38,43]. 58% conversion of ethane, 10.3% of CO_2, and 21.9% ethylene yield were achieved over these systems at 700 °C [43]. The conversion of ethane in these studies was higher relative to the thermodynamic equilibrium values of ethane conversion alone due to a significant contribution of secondary reactions [44]. Relatively low selectivity to ethylene showed a significant contribution to the direct ethane dehydrogenation resulting in high hydrogen production [38,43].

Mo_2C supported on SiO_2 was found to be an effective catalyst for the dehydrogenation of ethane to ethylene in the presence of CO_2. The selectivity to ethylene at 600-650 °C was 90–95% at an ethane conversion of 8–30%. At higher temperatures, dry reforming of ethane penalized ethylene yield. It is assumed that Mo oxycarbides formed in the reaction between CO_2 and Mo_2C play an important role in ethane activation [45]. Recently, a Mo-containing catalyst was reported for ODH-CO_2 but again only at 600 °C with relatively modest performance[30,46]. Oxygen from CO_2 appears crucial in cleaving the ethane C-C bond, increasing ethylene production. The addition of a Fe promoter accelerated the formation of surface oxygen species and stabilized them from reduction by ethane, leading to a shorter induction period, higher ethylene yield, and improved stability [30]. However, the main problems with Mo_2C catalysts operating at high temperatures remain the coking, sintering of the active Mo-species from cycle to cycle, and a significant contribution of the dry reforming reaction.

In order to design a stable at high-temperature Mo_2C-supported catalyst, we propose a different approach consisting of the utilization of MoS_2 precursors in place of oxides and embryonic zeolites (EZ) [47] as support in place of silica or alumina. An advantage of embryonic zeolites is the high surface area with a significant micropore volume resulting in the good dispersion and accessibility of all types of active sites [48]. In addition, EZ undergoes changes in surface area after the first heating cycle above 600 °C [48], which stabilizes the metal against sintering while keeping the active sites still accessible for the small molecules. After the first surface reduction, substantially no changes occur with these materials upon consecutive thermal cycles. In this context, the embryonic zeolites as support could also stabilize the formed molybdenum carbide phase at high temperatures. However, the aging of EZ zeolite is a long process, what may lead to the agglomeration of MoO_x-oxides species before carburization. In order to limit the agglomeration of the MoO_x species during the first heating cycle, the idea was to use a MoS_2-precursor supported on EZ. Supported sulfides, especially MoS_2, are also known for CO_2 hydrogenation at high-pressure [49], but using MoS_2 for oxidative or non-oxidative ethane dehydrogenation was never reported to the best of our knowledge.

This work reports the preparation of a novel thermally stable Mo-based catalyst supported on EZ carriers from a MoS_2 – precursor (Mo_2C@EZ), its comprehensive characterization, and catalytic performances in ODH-CO_2 of ethane.

Experimental section

2.1. Preparation of EZ carriers

An all-silica (EZ_{Si}) and an aluminosilicate ($EZ_{Al\text{-}Si}$) embryonic zeolites were used as carriers in all experiments.

The initial gel composition for the EZ_{Si} synthesis was 9 TPAOH:0.25 Al_2O_3:25 SiO_2:430 H_2O:100 EtOH, and for $EZ_{Al\text{-}Si}$, 9 TPAOH:25 SiO_2:430 H_2O:100 EtOH where TPAOH stands for tetrapropylammonium hydroxide [47]. A typical preparation procedure includes mixing the TPAOH solution (20% in water, Alfa Aesar) with distilled water. In the case of synthesis of the embryonic zeolite $Al_2(SO_4)\cdot 18\ H_2O$ (Sigma-Aldrich,98%) was subsequently added and the system homogenized by stirring. Tetraethyl orthosilicate (TEOS Sigma-Aldrich, 98%) was then added, and the mixture stirred for 6 h leading to the formation of water clear homogeneous sol. The solid product was recovered by freeze-drying (−94 °C under vacuum). The recovered solids were ion-exchanged with 0.5 mol ammonium nitrate solution, washed with distilled water, and dried under air. The resulting samples are referred to as $EZ_{Al\text{-}Si}$ and EZ_{Si}. A ZSM-5 (Si/Al=47.6) provided by Tosoh was used as a reference catalyst.

1.2.Metal loading and sulfidation

Mo oxide-decorated catalysts were prepared by incipient wetness impregnation on the embryonic zeolite carriers. The samples were loaded with 5 wt. % of Mo and denoted as $EZ_{Al\text{-}Si}$-5%Mo, EZ_{Si}-5%Mo, and ZSM-5-5%Mo. $(NH_4)_6Mo_7O_{24}\cdot 4H_2O$ (Alfa Aesar, 99%) was used as a source of Mo. After drying at room temperature, all samples were calcined at 550 °C for 5h in static air.

Mo sulfidation was performed under an H_2S/H_2 gas flow (30 ml/min, 10 vol%H_2S). 300 mg of the pelletized sample (35/45 mesh) was loaded in a Pyrex reactor, first heated under an N_2 flow at 140 °C for 2 h, then at 350 °C (2,8 °C·min^{-1} ramp rate) for 2 h under an H_2S/H_2 flow, cooled down to 180 °C and finally under a flow of dry N_2 to room temperature and kept there for 3 h. The samples were denoted $EZ_{Al\text{-}Si}$-5%MoS_2, EZ_{Si}-5%MoS_2, and the reference ZSM-5-5%MoS_2.

2.3 Physicochemical characterization

The powder X-ray diffraction (PXRD) patterns were recorded on a PANalytical X'Pert Pro diffractometer using the Cu Kα radiation (λ = 1.5418 Å). The scanning electron micrographs were collected on a MIRA-LMH (Tescan) SEM equipped with a field emission gun.

Nitrogen physisorption was performed on a Micromeritics ASAP 2020 surface area analyzer. The calcined samples were analyzed after degassing at 300 °C. The microporous volume (V_{mic}, $cm^3\cdot g^{-1}$) and the external surface area (S_{ext}, $m^2\cdot g^{-1}$) were obtained from the t-plot method based on the Harkins−Jura equation.

All ^{27}Al NMR measurements were done with 4 mm (o.d.) zirconia rotors spun at 14 kHz on a Bruker Avance 400 spectrometer operating at 100.6 MHz. ^{29}Si MAS NMR was recorded

on a Bruker Avance 500 spectrometer operating at 130.3 MHz. TMS was the reference for ^{29}Si, while a 1M $Al(NO_3)_3$ solution was used for ^{27}Al. The quantification of the spectra was done by integrating the peaks using the Dmfit program.

The formation of the Molybdenum oxide and sulfide phases was monitored by Raman spectroscopy. The Raman spectra were acquired with a green laser at 532 nm (Jobin Yvon Labram 300 confocal Raman spectrometer coupled to a microscope and CCD detector). Both accumulation time and laser power were adjusted for the samples (embryonic zeolites after metal loading: 40-60 s accumulation 3 times at 50% laser power; after sulfidation: 15-25 s accumulation 3 times at 1% laser power).

Pyridine adsorption monitored by IR spectroscopy was selected to evaluate the acidity. The spectra were collected on a Nicolet Magna 550 FTIR spectrometer equipped with a DTGS detector at a 4 cm^{-1} optical resolution with one level of zero filling for the Fourier transform. Prior to measurement, each sample was ground and pressed into a self-supporting disc (diameter: 2 cm, approximately 5 $mg \cdot cm^{-2}$) and activated in a vacuum (ca. 10^{-6} hPa) at 450 °C for 2 h at 2 $°C \cdot min^{-1}$. After cooling to room temperature, a spectrum was recorded as a reference. A pressure of 1.33 hPa of pyridine was established in the cell at room temperature till saturation was reached. The wafer was then heated to 100 °C for 15 min to facilitate pyridine diffusion in the whole disc. Successive evacuations were performed at 100, 150, 200, 250, 300, and 350 °C at 15 min intervals, and spectra were recorded at each step. All spectra were normalized to a 2.5 $mg \cdot cm^{-2}$ wafer. The number of acidic sites was determined using the areas of the bands at 1450 cm^{-1} (Lewis) and 1545 cm^{-1} (Brønsted). The molar extinction coefficients (ε) used for quantification were ε1545 (B-pyridine) = 1.8 $cm \cdot \mu mol^{-1}$, ε1455 (L-pyridine) = 1.5 $cm \cdot \mu mol^{-1}$ [47]. The OMNIC software program was used for data processing.

Thermogravimetric analysis (TGA) was carried out with a SETSYS SETARAM analyser. The temperature was increased from 30 to 800 °C at 5 °C/min in reconstituted (80 % N_2 + 20 % O_2) dry air (40 mL/min).

2.4 Catalytic test

300 mg of the 100–400 µm fraction was used for all the CO_2 oxidative ethane dehydrogenation tests. Before the reaction, all the catalysts were heated at 300 °C under reactants flow for 2 hours, as the accuracy of flow rates was verified. The catalysts were brought to the reaction temperature under a flow of reactants at a 10 °C/min ramp rate. After the reaction, the reactor cooled down to room temperature under a dry N_2 flow.

The effluents were analyzed online with a gas chromatograph (Interscience Compact GC) equipped with two thermal conductivity detectors (TCD), and a one flame ionization detector (FID). A Molsieve 5A, Rt-QBond, Rtx-1 were used to separate light gases (H_2, N_2, CO, CO_2),

light hydrocarbons (CH_4, C_2H_4, C_2H_6), and aromatics (from benzene till naphthalene), respectively. In all the experiments, N_2 was used as an internal standard to measure conversion and establish mass balance (Table S1). The mass balance in all the reported experiments was at least 99% (Table S1).

The tests were performed with a $C_2H_6/CO_2/N_2$= 49.5/36.5/14 (vol.%) mixture in the temperature range 700-800 °C, at atmospheric pressure with a weight hourly space velocity WHSV= 5.9 h^{-1} ($g_{C2H6}/g_{catalyst} \times h$).

In order to reveal the catalytic impact of the catalyst on the reaction yield, a blank test without any catalyst was performed under the same operating conditions (same linear velocity, same temperature, same total and partial pressure of the reagents). In the blank test C2 (ethane), N_2, and CO_2 were co-fed in the same ratio as in the catalytic reaction ($C_2H_6/CO_2/N_2$=49.5/36.5/14 (vol.%)). The blank test without a catalyst is referred to in the text as a thermal process ("thermal").

Ethane conversion (C_2 conversion), ethylene selectivity (C_2= selectivity), and CO selectivity (CO selectivity) were obtained as follows; the sum of the selectivities of the C3-C6 fraction and aromatics was labeled heavies:

$$Conversion(i) = \frac{C_{inlet}(i) - C_{outlet}(i)}{C_{inlet}(i)} \cdot 100\%$$

$$Carbon\ selectivity\ (i) = \frac{F(i)}{\sum F(i)} \cdot 100\%,$$

$$where\ F(i) - mol\ \ of\ the\ C\ in\ the\ product\ compound$$

A techno-economic analysis was done using an Aspen Plus simulator to compare our results with those typical of ethane steam cracking from the literature. The simulations were for a typical industrial-scale capacity of ethylene production of 1000 kt/year. The physical property databanks and methods as well as ASPEN Plus® models used are summarized in Table S2.

2. Results and discussion

3.1. Characterization of the catalysts

X-ray diffraction (XRD) indicates that on all samples, the embryonic carrier and the supported metal phase are X-ray amorphous (Fig. 1a), and EDX mapping indicates the metal is uniformly distributed on the EZ (Fig.1b).

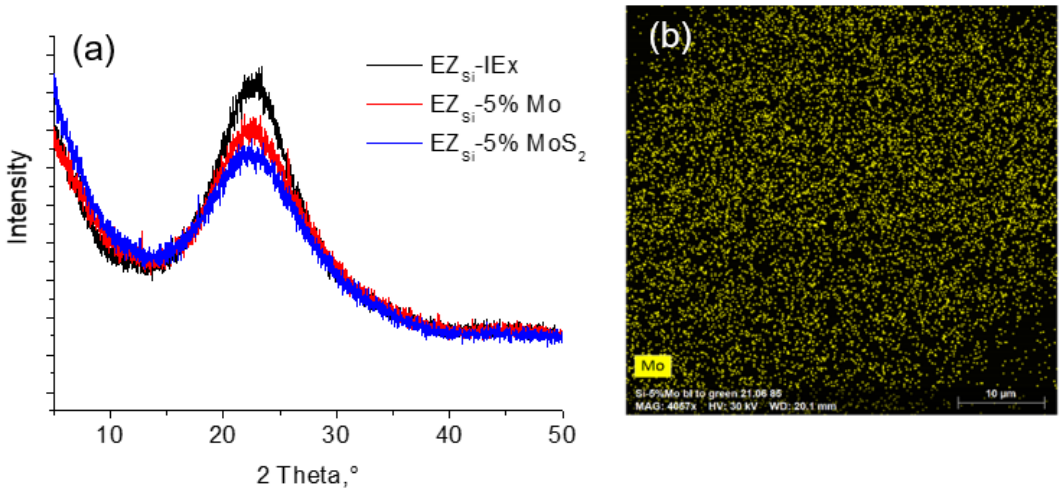

Fig. 1. a) XRD patterns of EZ_{Si}-IEx, EZ_{Si}-5%Mo, EZ_{Si}-5%MoS_2; b) EDX elemental mapping of Mo in EZ_{Si}-5%Mo.

The 77-K nitrogen sorption-desorption isotherms of the EZ carriers (Fig.2a) and the corresponding Mo- and MoS_2 – derivatives (Fig.2b) show the Type IV isotherms. The mesoporosity is attributed to the intercrystallite spaces between the embryonic units and is observed in all the cases. After impregnation with the metal precursor, micropore volume drops from about 90 cm^3/g to 70 cm^3/g for the Al-containing embryonic sample (EZ_{Al-Si}) and to 45 cm^3/g for all-silica embryos (EZ_{Si}). Mesopore volume decrease is observed only to a very small extent after each treatment for the catalysts. The results show that the metal precursors are mainly located in micropores of the supports.

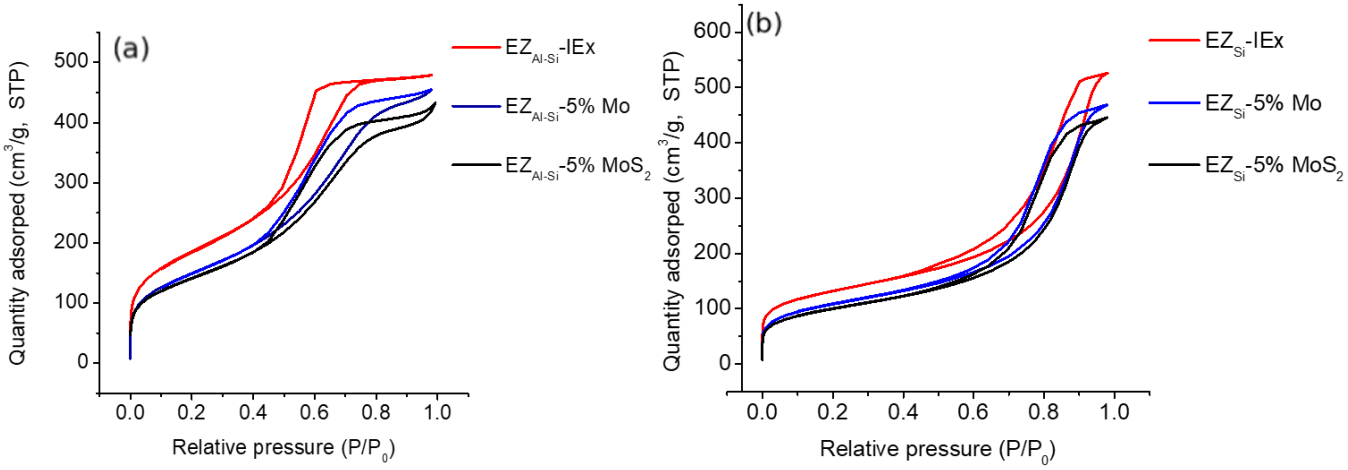

Fig. 2. N_2 adsorption-desorption isotherms: a)EZ_{Al-Si}-based; b)EZ_{Si}-based.

Raman spectroscopy was used to identify the nature of the metal phase in the EZ-supported catalysts (Fig.3). The spectrum of EZ_{Si}-5%Mo shows a wide band with two overlapping peaks at 990 cm^{-1} and 950 cm^{-1} and two better-resolved bands at 854 cm^{-1} and 821 cm^{-1}. These bands can be assigned to polymolybdates (950 cm^{-1}, 854 cm^{-1})[50] and α-MoO_3 (990 cm^{-1}, 821 cm^{-1}) [51] phases. In contrast, the EZ_{Al-Si}-5%Mo spectrum displays only an intense

band at 990 cm^{-1} with a shoulder at 854 cm^{-1}. We assume that both phases are also present on the latter catalyst, the polymolybdate phase being predominant.

The band at 480 cm^{-1} [52] corresponds to Si-O stretching in the SiO_2 tetrahedra and is attributed to 4-membered rings often reported at 472 cm^{-1} [53]. Both, EZ_{Si}-IEx and EZ_{Al-Si}-IEx display low-intensity bands around 970 and 1035 cm^{-1}. The 970 cm^{-1} band is assigned to Si–O stretching vibrations in terminal Si–OH groups [54], while the 1035 cm^{-1} band is characteristic for the stretching of alkyl chains of the protonated nitrogen atom of the organic template.

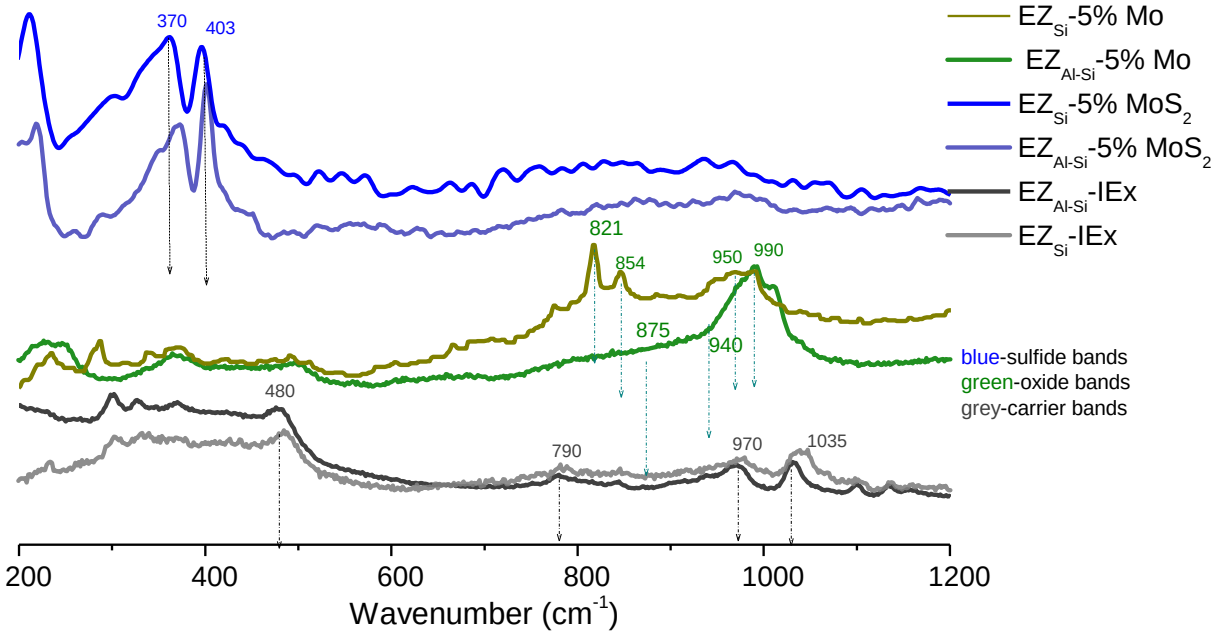

Fig. 3. Raman spectrum of EZ decorated with molybdenum oxide and sulfide phases.

The conversion of the oxide to the sulfide phase can also be monitored by Raman spectroscopy. Bands at 370 and 403 cm^{-1} are attributed to 2H-MoS_2 phase [55,56]. The wideband with a maximum of about 230 cm^{-1} is characteristic of silica tetrahedra in a bulk SiO_2 phase and remains unchanged after full oxide conversion.

The high-temperature stability of the catalyst carrier is studied by solid-state ^{27}Al and ^{29}Si NMR. The nature of the silicon environment in the parent all-silica EZ and Mo loaded after one calcination at 550 °C and subsequent calcination at 550 °C and at 700 °C is presented in Fig. 4a. All spectra display large peaks centered around –110 ppm, and the CP MAS spectrum exhibited a low resolved peak around -100 ppm. Only the parent contains a relatively large amount of Q^3 species. Small amounts of Q^2 species (-97 ppm) can be observed in EZ_{Si}-IEx and EZ_{Si}-5%Mo-550. All spectral deconvolutions are summarized in Table 1. They indicate that metal impregnation increases the number of Q^4 units along with a full disappearance of the Q^3 and Q^2's.

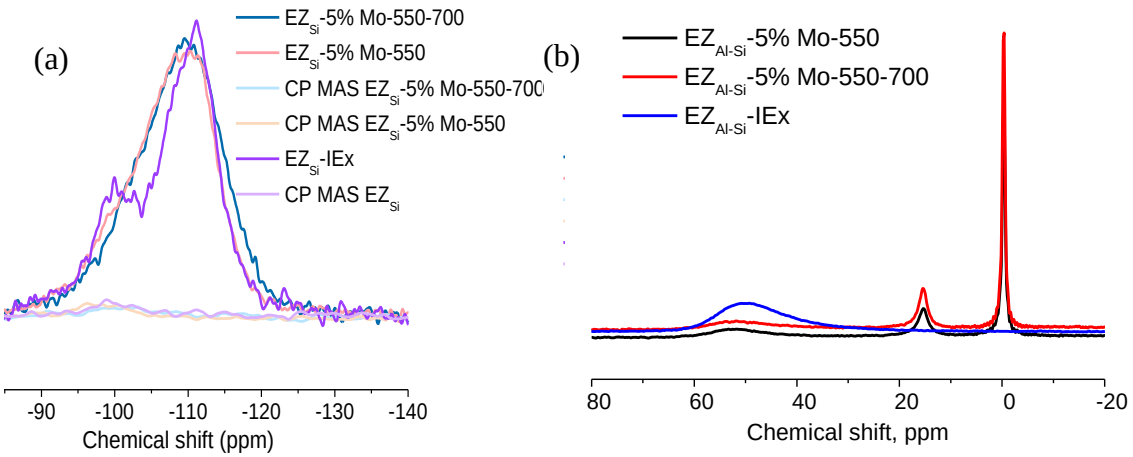

Fig. 4. Solid-state NMR analysis of the parent materials after ion exchange and Mo-loading: a) ^{29}Si NMR (1pulse) and CP MAS spectra; b) ^{27}Al NMR spectra.

Table 1. Relative percentage of Q^2, Q^3, and Q^4 silicon environments in EZ_{Si}-parents and calcined derivatives.

Sample	Q^2	Q^3	Q^4
EZ_{Si}-IEx	7	48	45
EZ_{Si}-5%Mo-550	2	22	76
EZ_{Si}-5%Mo-550-700	-	27	73

During the high-temperature treatment of silica-alumina embryos (550 °C or consecutive calcination at 550 and 700 °C) after Mo loading, Al is extracted from tetrahedral positions, Fig.4b while the parent, ion-exchanged with NH_4NO_3, does not contain any octahedral Al. The calcined samples loaded with 5 wt.% Mo, three types of aluminum coexist (Al^{IV}, Al^{VI}, and $Al_2(MoO_4)_3$), witnessing the catalysts alteration at high temperatures.

3.2. Catalytic performances

It is known that above 650 °C, MoO_x and MoS_2 species react with hydrocarbons to produce Mo_2C [57,58]. The mechanism of Mo_2C phase formation from MoS_2 in the presence of CH_4 and H_2 is described [59]. The carbide formation from MoO_3 under C_2H_6 and C_4H_{10} is also reported [60]. In this contribution, the active Mo_2C phase is obtained *in situ* by subjecting the Mo-containing precursor in a contact with the mixture of C_2H_6/CO_2 =1/0.74 at 700 °C. The hypothesis on Mo_2C formation is based on the typical profile of the TG curve [61] and on the observation of the characteristic bands for the graphitized carbon in Raman spectra synthesized with non-methane carburization agent [62, 63]. The TGA curves of the spent Mo_2C-containing samples demonstrated a slight weight increase up to 470 °C due to the oxidation reaction of Mo_2C to MoO_3 (Fig.S3). However, the analysis of Mo_2C on the spent catalysts by Raman spectroscopy is a difficult task. The sulfidic form on the precursor is confirmed by the two bands

around 370 and 403 cm^{-1} (Fig.5), both bands are disapered on the spent Mo_2C-containing samples. That shows the transformation of the MoS_2 -species to a different species. In addition, two new intense bands are detected in the region of C-C vibrations – (band D) at 1350 and (band G) 1600 cm^{-1} on the sample after the reaction. They are typically attributed to the graphitized carbon (Fig.5) [64]. The intensity ratio of G (1580 cm^{-1}) to D (1350 cm^{-1}) band reflects the graphitization degree of catalysts [63].These data suggest that the excess of methane led to the formation of graphitic carbon with the characteristic bands at 1350 and at 1600 cm^{-1}, which are also typically observed when the Mo_2C phase is formed [63]. The same covering of Mo-C bands was demonstrated under ethane, while XRD confirmed the formation of the claimed phase [63].

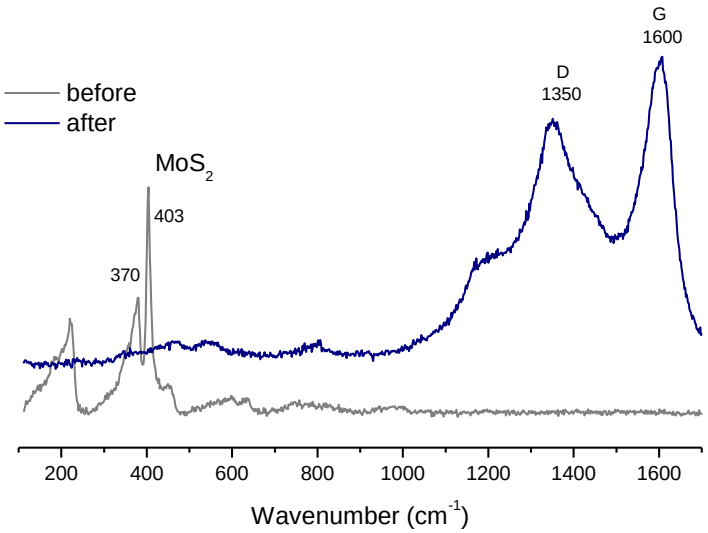

Fig. 5. Raman spectrum of embryonic zeolite decorated with sulfide phase before and after the catalytic test at 700 °C over EZ_{Si}-5%$(Mo_2C)_S$.

3.2.1. Impact of Mo-precursor:MoO_x vs MoS_2

Thermal, *i.e.*, the non-catalytic transformation of the mixture of ethane and CO_2 at 700 °C, results in ethane to ethylene conversion level, which is close to the thermodynamic equilibrium, with the ethylene selectivity above 95%. However, only a very limited CO_2 conversion is observed in this case. In contrast, the presence of the Mo_2C-supported on embryonic zeolite catalyst, formed from MoS_2 or MoO_x -precursors (EZ_{Si}-5%$(Mo_2C)_S$ or EZ_{Si}-5%$(Mo_2C)_O$), leads to a significantly higher CO_2 conversion. One can also see that the EZ_{Si}-5%$(Mo_2C)_S$ from MoS_2-precursor performs CO_2 transformation substantially without decreasing the ethane conversion in comparison with the one in the thermal process (Fig.6a). Moreover, the selectivity to ethylene is higher (Fig.6b). In contrast, the MoO_x-derived catalyst displays not only lower CO_2 conversion in comparison with the MoS_2-derived catalyst but also significant activity in ethylene hydrogenation back to ethane and very high methane selectivity (Fig.6a, Fig.6b).

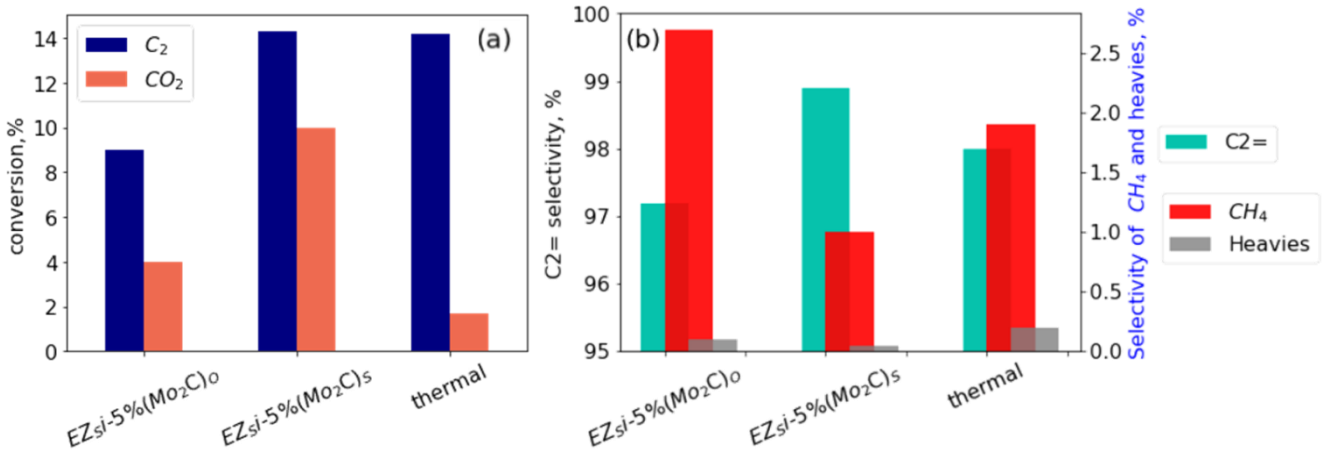

Fig. 6. ODH-CO_2 of ethane on EZ_{Si}-5%(Mo_2C)$_O$, EZ_{Si}-5%(Mo_2C)$_S$, and without catalyst: a) conversion of CO_2 and ethane; b) selectivities to the products (coke-free basis, 700 °C, C_2H_6/CO_2=1/0.74, WHSV = 5.9 h^{-1}, average level for 2-5 hours-on-stream).

The results summarized in Table S3 show that only a few by-products are produced in all the cases. The MoS_2-derived catalyst also demonstrates higher stability than the MoO_x-derived one (Fig.S1) and the highest selectivities in all cases. Therefore, the MoS_2-derived catalyst was selected for further investigation.

3.2.2. Impact of the catalyst carrier

The performances in the ODH-CO_2 reaction of a series of MoS_2-derived catalysts supported on EZ of different acidity (EZ_{Si}-5%(Mo_2C)$_S$, $EZ_{Al\text{-}Si}$-5%(Mo_2C)$_S$, ZSM-5-5%(Mo_2C)$_S$) was evaluated. An embryonic zeolite and a conventional ZSM-5 with a crystal size of about 1 µm with a similar Si/Al atomic ratio were used for the study. The Bronsted acidity (BAS) and the Lewis acidity (LAS) of the supports before metal impregnation was assessed by FTIR adsorption of pyridine (Table 2). While the siliceous EZ_{Si} did not display any acidity, the Al-containing embryonic zeolite ($EZ_{Al\text{-}Si}$) showed some acid properties (Table 2). As expected, the highest acidity was measured on the zeolite carrier (ZSM-5).

Table 2. Acid site concentration on ZSM-5 and Al-containing embryonic zeolite measured by FTIR with pyridine probe molecule.

Sample	LAS, µmol/g	BAS, µmol/g
ZSM-5 (Si/Al=47)	235	1094
$EZ_{Al\text{-}Si}$ (Si/Al=43)	57	185

The initial CO_2 and C_2H_6 conversions on the catalysts prepared on acidic support (ZSM-5-5%$(Mo_2C)_S$ and $EZ_{Al\text{-}Si}$-5%$(Mo_2C)_S$) were significantly higher than on siliceous one (Fig. S2). In the case of ZSM-5-5%$(Mo_2C)_S$, ethane and CO_2 conversions were 37 % and 30 %, respectively. However, the main products were coke and aromatics, leading to rapid deactivation: down to 18% C_2H_6 and 13 % CO_2 after 140 min-on-stream, respectively. The result showed that the strong acidity of the support, which is typical for the zeolites is not desirable and leads to many side reactions.

The embryonic zeolite with a bulk Si/Al ratio close to the ZSM-5 one showed lower acid site concentration and, as a consequence, slower deactivation in comparison to the one on ZSM-5 support. It should be mentioned that the selectivity patterns on the Al-containing $EZ_{Al\text{-}Si}$-5%$(Mo_2C)_S$ catalyst and on Al-free EZ_{Si}-5%$(Mo_2C)_S$ catalysts looked more similar. One of the potential advantages of the Al-containing embryonic zeolite is the higher activity in CO_2 hydrogenation. However, higher coke content, in addition to higher methane selectivity, makes the acidity a disadvantage in this reaction (Fig.S3).

3.2.3. Performance of Al-free EZ_{Si}-5%$(Mo_2C)_S$ in ODH-CO_2 of ethane

The selected purely silicious EZ_{Si} material showed to be advantageous in the dispersion and stabilization of Mo_2C while preventing deactivation due to coke formation (Fig.7a, Fig.S3). Indeed, MoS_2-precursor supported on EZ extends the operating temperature range of Mo_2C catalysts compared to previously published results [36,37,45], in addition to suppressing the unwanted side reactions of methanation and dry-reforming. Remarkably, the selectivity to ethylene is even higher at the same process temperature than in the thermal process (Fig.7b).

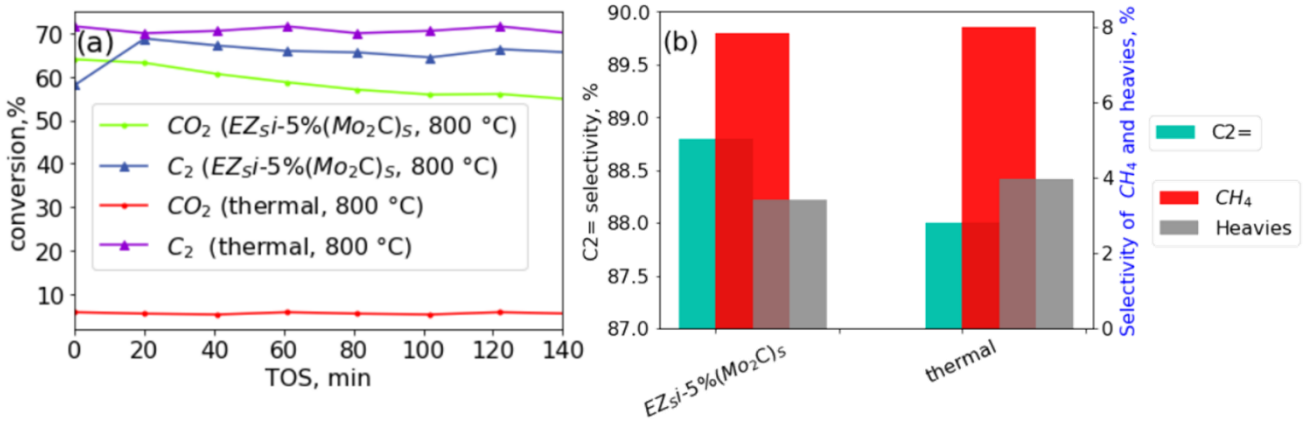

Fig. 7. ODH-CO_2 of ethane (C2) on EZ_{Si}-5%$(Mo_2C)_S$ and without catalyst: a) conversion of CO_2 and ethane as a function on time-on-stream; b) selectivities to the products (coke-free basis, T =800 °C, P = 1 atm, C_2H_6/CO_2 = 1/0.74, WHSV =5.9 h^{-1}).

The difference in ethane's catalytic and thermal conversion is due to some ethylene hydrogenation. Although the activity in ethylene hydrogenation is significantly lower on the catalyst than the one in CO_2 conversion to CO, it is worth comparing the selectivity at different temperatures at the same level of conversion.

The selected catalyst (EZ_{Si}-5%$(Mo_2C)_S$) was tested at different temperatures, and its performance was compared with the thermal (without catalyst) transformation of ethane in the presence of CO_2 (Fig. 8). Due to some partial hydrogenation, the apparent ethane conversion level at the same temperature was slightly lower than in the thermal process (Fig.S4). In order to compare the results, the data were linearly extrapolated to the same level of conversion. Three conversion levels of ethane were selected for the comparison: low conversion (15%), mid conversion (40%), and high conversion (66%). In contrast to literature data on Mo_2C type of materials [45], one can see that at about 50% of CO_2 conversion to CO (reverse water-gas-shift reaction), the methanation and the dry reforming remained insignificant in the studied system (Fig. 8). In all cases, the ethylene selectivities in -CO_2 of ethane were found very close between catalytic and non-catalytic processes. The impact on ethylene selectivity did not exceed 1-3 % for all the conversion levels of ethane, which could be considered insignificant. One can see that the presence of catalyst allows achieving a 50% conversion level of CO_2 without decreasing the selectivity to ethylene in comparison with the thermal process at the conversion of ethane up to 66% (Fig.8). All the results were obtained in the temperature range 700-800 °C what is the industrially relevant temperature range for the ethane cracking. A detailed comparison with the ethane cracking of the obtained catalyst performance is given below.

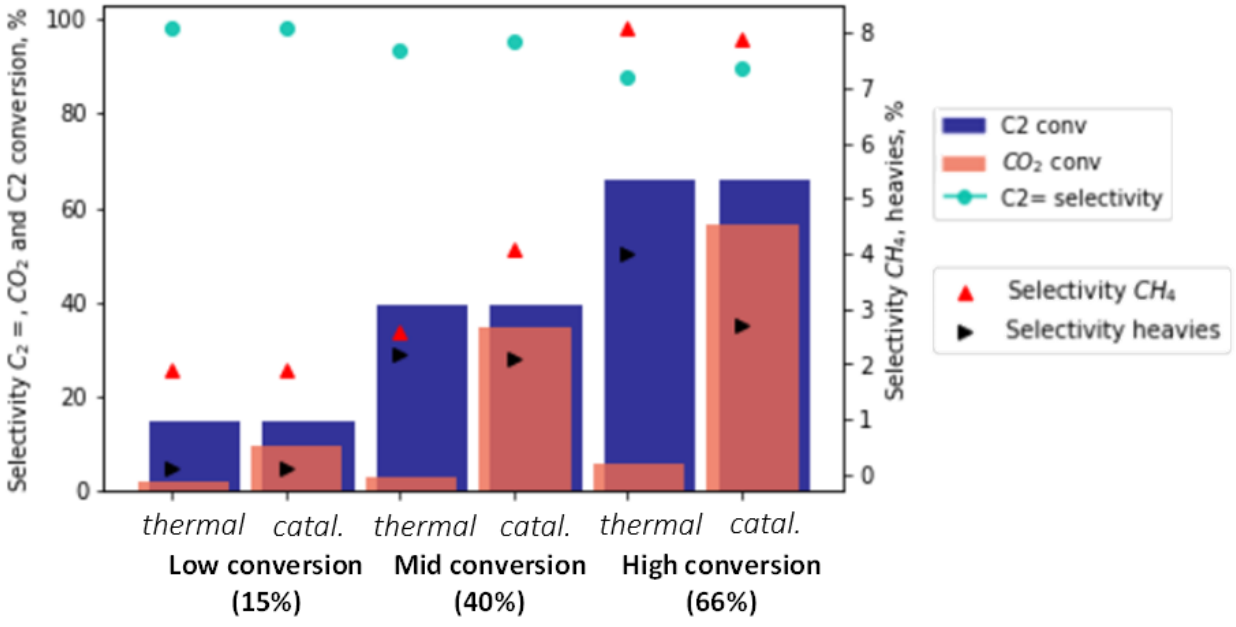

Fig.8. Comparison of catalytic (EZ_{Si}-5%$(Mo_2C)_S$) and thermal performances in ODH-CO_2 of

ethane at the same conversion level of ethane (coke-free basis, C_2H_6/CO_2=1/0.74, WHSV = 5.9 h^{-1}).

3.3. Techno-economical analysis of the ODH-CO_2 process based on an EZ_{Si}-5%$(Mo_2C)_S$ catalyst

As mentioned in the introduction section, the emerging technological solutions aim to produce ethylene from ethane with lower CO_2 emissions in comparison with an ethane cracker.

The endothermic cracking of ethane (its C-C and C-H bonds require dissociation energies of 345 and 413 kJ/mol, respectively) to ethylene yield is limited. It requires high temperature and leads to the formation of side products such as aromatics and light gaseous. The catalytic conversion of ethane to ethylene in the presence of an oxidant is a potential solution to the problems outlined above. The ODH-E technology recently developed by Linde/Clariant reports CO_2 emissions reductions in the 23-32% range compared to conventional steam cracking [18]. The EcoCatalytic's CL-ODH technology also claims a 64% substantial reduction in CO_2 emissions compared to a state-of-the-art ethane steam cracker of the same capacity [22]. In the case of the state-of-the-art ethane steam cracker, hydrogen is the by-product. Such hydrogen could alternatively be used as a fuel for heat generation, leading to overall CO_2 emission reduction.

In such a broader context, oxidative dehydrogenation of ethane in the presence of CO_2 (ODH-CO_2) is a promising economical and environmental alternative. This process directly utilizes hydrogen to transform CO_2 into CO, which could further be used as the precursor for producing valuable chemicals, mitigating CO2 emissions while simultaneously achieving ethane dehydrogenation. This process can not only reduce CO_2 emission but also simplifies production slate processing by reducing CH_4 and heavies production.

Steam cracking proceeds through free-radical mechanisms [65], which are inherently characterized by a vast number of species and reactions leading to wide product distribution. Moreover, in steam crackers, acetylene is a by-product. Typically, the acceptable acetylene contaminant level in polymer grade ethylene products is 1 ppmv or lower. Since acetylene will fractionate with ethylene, it needs to be removed before the C2 fractionation step. An acetylene hydrogenation unit is often required to convert it to ethylene. Consequently, the downstream processing of a steam cracker requires multiple separation units, as shown in Fig. S5a.

In a state-of-the-art ethane steam cracker, the traces of CO are hydrogenated to CH_4, and the unconverted H_2 is of low grade with a significant amount of methane. The ODH-CO_2 process results in a significant amount of CO, significantly lower methane production, and some remaining hydrogen. So, the light end from an ODH-CO_2 could be considered as syngas, which after an adjustment of hydrogen content, could be directly suitable for MeOH synthesis.

ODH-CO_2 results in a lower amount of heavies, with almost no C_3 fraction and no acetylene, detected in the effluent of the reactor, as seen in Table 3. That is very interesting for separation and, eventually, for the energy balance. On the other hand, the C_2/CO_2 fraction should not be necessarily separated and could be recycled back to the reaction session as a feedstock (Fig S5b).

Table 3. Comparison of steam cracking (SC) of ethane and ODH-CO_2.

	SC of ethane [66], 845 °C-outlet	ODH-CO_2 [this work]
Ethane Conversion (%)	65.0	66.1
Carbon Yield (dry mol%)		
CO	0.00	27.34
CO2	0.00	20.71
CH_4	3.40	4.81
C_2H_2	0.50	0.00
C_2H_4	56.10	27.29
C_2H_6	35.00	19.46
C_3H_6	1.20	0.00
C_3H_8	0.10	0.00
C_4H_6	2.10	0.00
C_4H_8	0.20	0.00
C_4H_{10}	0.20	0.30
C_5's	0.60	0.10
Aromatics (benzene, toluene)	0.60	0.08

Figure 9 highlights the unit operations of a conventional SC plant and an ODH-CO_2 plant. The ODH-CO_2 requires 50% less unit operations compared to an ethane cracker. One can see that ODH-CO_2 may bring significant advantages in terms of investment costs and separation duties and therefore reduce CAPEX and OPEX.

Regarding energy consumption, ethylene production via steam cracking of ethane is very energy consuming: producing 1 ton of ethylene typically requires **21 GJ** of thermal energy (process energy consumed in pyrolysis and separation) and results in approximately **1.2** tons of CO_2 emissions [5]. In our case, the simulation of the ODH-CO_2 process indicates an energy consumption of **17.4 GJ** of thermal energy to produce 1 ton of ethylene and **consumes 1,09 tons of CO_2**. Therefore, if ODH-CO_2 is implemented based on the current catalytic results, the reduction of CO_2 would be up 109% in comparison with the state-of-the-art ethane cracker making the technology CO_2 negative.

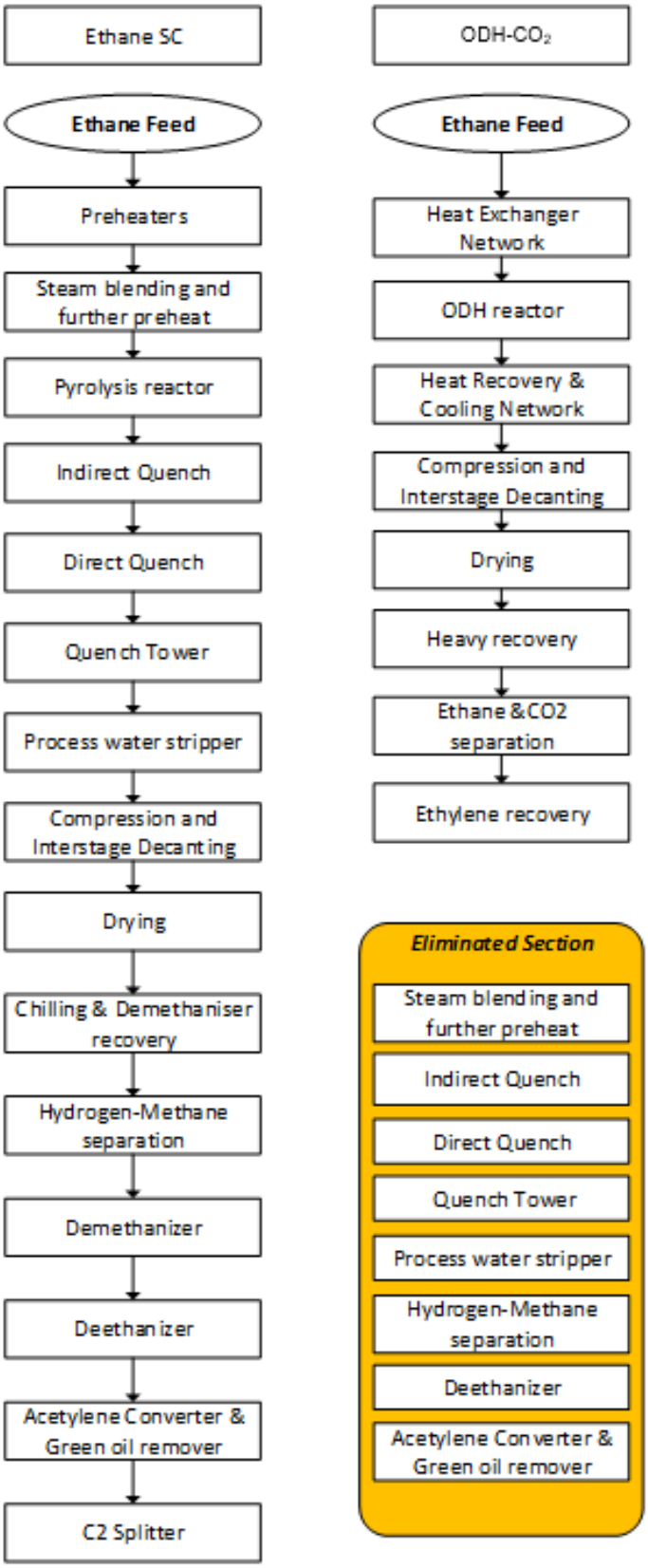

Fig 9. Comparison in term of unit operations between SC and OHD-CO_2 ([55])

3. Conclusions

Embryonic zeolites show potential as supports for Mo_2C active species in ODH-CO_2. Supported metal sulfides proved to be efficient precursors of the Mo_2C active phase, which allows the designing of novel thermally stable and highly active catalysts for CO_2 hydrogenation in co-processing with alkenes. This "sulfide" route shows a clear advantage over the "oxide" one and requires only about 5 wt.% of Mo.

Although a detailed formation mechanism from MoS_2 to Mo_2C is still under investigation, it seems that MoS_2 supported on embryonic zeolites prevents sintering of the Mo-species during the carbide formation and results in a more active and stable catalyst for ODH-CO_2 of ethane. The latter allows operating at higher temperatures, avoiding dry reforming and methanation side reactions while producing more selectively ethylene.

The supported Mo_2C displays a good activity in CO_2 hydrogenation without negatively impacting the thermal C_2 conversion to ethylene at a conversion up to 66%. The resulting ODH-CO_2 process could lead to a potentially promising CO_2-negative technology with a much-reduced separation section due to a lower amount of heavies, no acetylene production, and better carbon efficiency. ODH-CO_2 thus brings significant advantages in terms of investment (CAPEX) and operating (OPEX) costs of a greener process.

Acknowledgments

This research was supported by TotalEnergies, the Industrial Chair ANR-TOTAL "NanoClean Energy" (ANR-17-CHIN-0005-01), and project NanoCleanEnergy$^+$ (Region Normandy).

CRediT authorship contribution statement

Vera Bikbaeva: Investigation, Methodology, Writing - Original Draft. **Nikolay Nesterenko:** Conceptualization, Supervision, Writing-review and Editing. **Thanh-Son Nguyen:** Investigation. **Stanislav Konnov:** Investigation. **Valentin Valtchev:** Conceptualization, Supervision, Writing-review and Editing.

Declaration of Competing Interest

The authors declare that they have no known competing financial interests or personal relationships that could have appeared to influence the work reported in this paper.

Appendix A. Supporting information

Supplementary data associated with this article can be found in the online version at doi:10.xxxx/xxxxxx.

References

[1] T.D. Foley, S.W. Sohn, Ethylene production by steam cracking of normal paraffins, WO2002036716A1, 2002.

[2] Ethylene production capacity globally 2025, Statista, Oxidative Dehydrogenation of Ethane Technology. https://www.statista.com/statistics/1067372/global-ethylene-production-capacity/ 2021 (accessed September 22, 2021).

[3] Ethylene Global Supply Demand Analytics Service, Wood Mackenzie. https://www.woodmac.com/ja/news/editorial/ethylene-global-supply-demand-analytics-service/ 2018, (accessed September 27, 2021).

[4] H. Zimmermann, R. Walzl, Ethylene, in: Wiley-VCH Verlag GmbH & Co. KGaA (Ed.), Ullmanns Encycl. Ind. Chem., Wiley-VCH Verlag GmbH & Co. KGaA, Weinheim, Germany, 2009: p. a10_045.pub3. https://doi.org/10.1002/14356007.a10_045.pub3.

[5] T. Ren, M. Patel, K. Blok, Olefins from conventional and heavy feedstocks: Energy use in steam cracking and alternative processes, Energy. 31 (2006) 425–451. https://doi.org/10.1016/j.energy.2005.04.001.

[6] Y. Yao, D.J. Graziano, M. Riddle, J. Cresko, E. Masanet, Understanding Variability To Reduce the Energy and GHG Footprints of U.S. Ethylene Production, Environ. Sci. Technol. 49 (2015) 14704–14716. https://doi.org/10.1021/acs.est.5b03851.

[7] A. Mohsenzadeh, A. Zamani, M.J. Taherzadeh, Bioethylene Production from Ethanol: A Review and Techno-economical Evaluation, ChemBioEng Rev. 4 (2017) 75–91. https://doi.org/10.1002/cben.201600025.

[8] E. Johnson, A carbon footprint of HVO biopropane, Biofuels Bioprod. Biorefining. 11 (2017) 887–896. https://doi.org/10.1002/bbb.1796.

[9] W. Vermeiren, N.V. Gyseghem, Procédé de production de produits de craquage par vapocraquage de bio-naphtha et bio-propane obtenus à partir de mélanges complexes d'huiles et de graisses existant à l'état naturel, EP3059295A1, 2016.

[10] F. Jamil, M. Aslam, A.H. Al-Muhtaseb, A. Bokhari, S. Rafiq, Z. Khan, A. Inayat, A. Ahmed, S. Hossain, M.S. Khurram, M.S. Abu Bakar, Greener and sustainable production of bioethylene from bioethanol: current status, opportunities and perspectives, Rev. Chem. Eng. 38 (2022) 185–207. https://doi.org/10.1515/revce-2019-0026.

[11] M. Zhang, Y. Yu, Dehydration of Ethanol to Ethylene, Ind. Eng. Chem. Res. 52 (2013) 9505–9514. https://doi.org/10.1021/ie401157c.

[12] A. Corma, G. Huber, L. Sauvanaud, P. Oconnor, Processing biomass-derived oxygenates in the oil refinery: Catalytic cracking (FCC) reaction pathways and role of catalyst, J. Catal. 247 (2007) 307–327. https://doi.org/10.1016/j.jcat.2007.01.023.

[13] K.M.V. Geem, T. Dijkmans, J.M. Anthonykutty, S.P. Pyl, A. Harlin, G.B. Marin, Production of Bio-Ethylene: Alternatives for Green Chemicals and Polymers, (2013) 23.

[14] Q. Yang, H. Zhou, P. Bartocci, F. Fantozzi, O. Mašek, F.A. Agblevor, Z. Wei, H. Yang, H. Chen, X. Lu, G. Chen, C. Zheng, C.P. Nielsen, M.B. McElroy, Prospective contributions of biomass pyrolysis to China's 2050 carbon reduction and renewable energy goals, Nat. Commun. 12 (2021) 1698. https://doi.org/10.1038/s41467-021-21868-z.

[15] E. Heracleous, A. Lee, K. Wilson, A. Lemonidou, Investigation of Ni-based alumina-supported catalysts for the oxidative dehydrogenation of ethane to ethylene: structural characterization and reactivity studies, J. Catal. 231 (2005) 159–171. https://doi.org/10.1016/j.jcat.2005.01.015.

[16] K. Chen, A. Khodakov, J. Yang, A.T. Bell, E. Iglesia, Isotopic Tracer and Kinetic Studies of Oxidative Dehydrogenation Pathways on Vanadium Oxide Catalysts, J. Catal. 186 (1999) 325–333. https://doi.org/10.1006/jcat.1999.2510.

[17] J.H. Kolts, J.P. Guillory, Composition of matter and method of oxidative conversion of organic compounds therewith, US4672145A, 1987.

[18] (124b) Oxidative Dehydrogenation of Ethane Technology, AIChE Academy. https://www.aiche.org/academy/conferences/aiche-spring-meeting-and-global-congress-on-process-safety/2020/proceeding/paper/124b-oxidative-dehydrogenation-ethane-technology,2020 (accessed September 22, 2021).
[19] C.A. Gärtner, A.C. van Veen, J.A. Lercher, Oxidative Dehydrogenation of Ethane: Common Principles and Mechanistic Aspects, ChemCatChem. 5 (2013) 3196–3217. https://doi.org/10.1002/cctc.201200966.
[20] F. Cavani, N. Ballarini, A. Cericola, Oxidative dehydrogenation of ethane and propane: How far from commercial implementation?, Catal. Today. 127 (2007) 113–131. https://doi.org/10.1016/j.cattod.2007.05.009.
[21] S.C. Arnold, A.M. Gaffney, R. Song, C.Y. Yeh, Process for producing ethylene via oxidative dehydrogenation (ODH) of ethane, US8519210B2, 2013.
[22] L.M. Neal, V.P. Haribal, F. Li, Intensified Ethylene Production via Chemical Looping through an Exergetically Efficient Redox Scheme, IScience. 19 (2019) 894–904. https://doi.org/10.1016/j.isci.2019.08.039.
[23] BASF, SABIC and Linde join forces to realize the world's first electrically heated steam cracker furnace. https://www.basf.com/global/en/who-we-are/sustainability/whats-new/sustainability-news/2021/basf-sabic-and-linde-join-forces-to-realize-wolds-first-electrically-heated-steam-cracker-furnace.html (accessed March 9, 2022).
[24] Petrochemical companies form Cracker of the Future Consortium and sign R&D agreement - Borealis, Borealisgroup. (2019). https://www.borealisgroup.com/news/petrochemical-giants-form-consortium-cracker-of-the-future-and-sign-agreement (accessed September 27, 2021).
[25] Dow and Shell demonstrate progress in joint technology development for lower CO2 emission crackers. https://nl.dow.com/en-us/news/dow-and-shell-electrified-cracker-lowers-emissions.html (accessed September 27, 2021).
[26] D. Wang, M. Xu, C. Shi, J.H. Lunsford, Effect of carbon dioxide on the selectivities obtained during the partial oxidation of methane and ethane over Li+/MgO catalysts, Catal. Lett. 18 (1993) 323–328. https://doi.org/10.1007/BF00765277.
[27] O.V. Krylov, A.Kh. Mamedov, S.R. Mirzabekova, The regularities in the interaction of alkanes with CO2 on oxide catalysts, Catal. Today. 24 (1995) 371–375. https://doi.org/10.1016/0920-5861(95)00061-J.
[28] O.V. Krylov, A.Kh. Mamedov, S.R. Mirzabekova, Oxidation of Hydrocarbons and Alcohols by Carbon Dioxide on Oxide Catalysts, Ind. Eng. Chem. Res. 34 (1995) 474–482. https://doi.org/10.1021/ie00041a007.
[29] K. Nakagawa, M. Okamura, N. Ikenaga, T. Suzuki, K. Nakagawa, M. Okamura, T. Suzuki, T. Kobayashi, T. Kobayashi, Dehydrogenation of ethane over gallium oxide in the presence of carbon dioxide, Chem. Commun. (1998) 1025–1026. https://doi.org/10.1039/a800184g.
[30] S. Yao, B. Yan, Z. Jiang, Z. Liu, Q. Wu, J.H. Lee, J.G. Chen, Combining CO_2 Reduction with Ethane Oxidative Dehydrogenation by Oxygen-Modification of Molybdenum Carbide, ACS Catal. 8 (2018) 5374–5381. https://doi.org/10.1021/acscatal.8b00541.
[31] A. Talati, M. Haghighi, F. Rahmani, Oxidative dehydrogenation of ethane to ethylene by carbon dioxide over Cr/TiO2–ZrO2 nanocatalyst: Effect of active phase and support composition on catalytic properties and performance, Adv. Powder Technol. 27 (2016) 1195–1206. https://doi.org/10.1016/j.apt.2016.04.003.
[32] M. Myint, B. Yan, J. Wan, S. Zhao, J.G. Chen, Reforming and oxidative dehydrogenation of ethane with CO2 as a soft oxidant over bimetallic catalysts, J. Catal. 343 (2016) 168–177. https://doi.org/10.1016/j.jcat.2016.02.004.
[33] A. Qiao, V.N. Kalevaru, J. Radnik, A. Martin, Oxidative dehydrogenation of ethane to ethylene over Ni–Nb–M–O catalysts: Effect of promoter metal and CO2-admixture on the performance, Catal. Today. 264 (2016) 144–151. https://doi.org/10.1016/j.cattod.2015.08.043.

[34] R. Koirala, O.V. Safonova, S.E. Pratsinis, A. Baiker, Effect of cobalt loading on structure and catalytic behavior of CoOx /SiO_2 in CO_2 -assisted dehydrogenation of ethane, Appl. Catal. Gen. 552 (2018) 77–85. https://doi.org/10.1016/j.apcata.2017.12.025.
[35] P. Thirumala Bai, S. Srinath, K. Upendar, T.V. Sagar, N. Lingaiah, K.S. Rama Rao, P.S. Sai Prasad, Oxidative dehydrogenation of ethane with carbon dioxide over Cr_2O_3/SBA-15 catalysts: the influence of sulfate modification of the support, Appl. Petrochem. Res. 7 (2017) 107–118. https://doi.org/10.1007/s13203-017-0182-5.
[36] T.A. Bugrova, V.V. Dutov, V.A. Svetlichnyi, V. Cortés Corberán, G.V. Mamontov, Oxidative dehydrogenation of ethane with CO_2 over CrO_x catalysts supported on Al_2O_3, ZrO_2, CeO_2 and $Ce_xZr_{1-x}O_2$, Catal. Today. 333 (2019) 71–80. https://doi.org/10.1016/j.cattod.2018.04.047.
[37] S.A. Theofanidis, C. Loizidis, E. Heracleous, A.A. Lemonidou, CO_2-oxidative ethane dehydrogenation over highly efficient carbon-resistant Fe-catalysts, J. Catal. 388 (2020) 52–65. https://doi.org/10.1016/j.jcat.2020.05.004.
[38] A. Bakhtyari, S. Zafarnak, H. Taghvaei, M.R. Rahimpour, A. Iulianelli, Simultaneous production of ethylene and hydrogen through carbon-dioxide-assisted conversion of ethane over cobalt-molybdenum catalysts, J. CO2 Util. 47 (2021) 101499. https://doi.org/10.1016/j.jcou.2021.101499.
[39] R.B. Watson, U.S. Ozkan, Mo Loading Effects over Mo/Si : Ti Catalysts in the Oxidative Dehydrogenation of Ethane, J. Catal. 208 (2002) 124–138. https://doi.org/10.1006/jcat.2002.3548.
[40] E. Heracleous, A.F. Lee, I.A. Vasalos, A.A. Lemonidou, Surface Properties and Reactivity of Al_2O_3-Supported MoO_3 Catalysts in Ethane Oxidative Dehydrogenation, 88 (2003) 47–53. https://doi.org/10.1023/A:1023534816277.
[41] X. Liu, C. Kunkel, P. Ramírez de la Piscina, N. Homs, F. Viñes, F. Illas, Effective and Highly Selective CO Generation from CO_2 Using a Polycrystalline α-Mo_2C Catalyst, ACS Catal. 7 (2017) 4323–4335. https://doi.org/10.1021/acscatal.7b00735.
[42] M.D. Porosoff, X. Yang, J.A. Boscoboinik, J.G. Chen, Molybdenum Carbide as Alternative Catalysts to Precious Metals for Highly Selective Reduction of CO_2 to CO, Angew. Chem. Int. Ed. 53 (2014) 6705–6709. https://doi.org/10.1002/anie.201404109.
[43] S. Zafarnak, A. Bakhtyari, H. Taghvaei, M.R. Rahimpour, A. Iulianelli, Conversion of ethane to ethylene and hydrogen by utilizing carbon dioxide: Screening catalysts, Int. J. Hydrog. Energy. 46 (2021) 19717–19730. https://doi.org/10.1016/j.ijhydene.2020.09.150.
[44] V. Bikbaeva, O. Perez, N. Nesterenko, V. Valtchev, Ethane oxidative dehydrogenation with CO_2 on thiogallates, Inorg. Chem. Front. (2022) 10.1039.D2QI01630C. https://doi.org/10.1039/D2QI01630C.
[45] F. Solymosi, R. Nemeth, The oxidative dehydrogenation of ethane with CO_2 over Mo_2C/SiO_2 catalyst, Cat Lett. 62 (1999) 197–200.
[46] W. Marquart, M. Claeys, N. Fischer, Conversion of CO_2 and small alkanes to platform chemicals over Mo_2C-based catalysts, Faraday Discuss. 230 (2021) 68–86. https://doi.org/10.1039/D0FD00138D.
[47] M. Akouche, J.-P. Gilson, N. Nesterenko, S. Moldovan, D. Chateigner, H.E. Siblani, D. Minoux, J.-P. Dath, V. Valtchev, Synthesis of Embryonic Zeolites with Controlled Physicochemical Properties, Chem. Mater. 32 (2020) 2123–2132. https://doi.org/10.1021/acs.chemmater.9b05258.
[48] K.-G. Haw, J.-P. Gilson, N. Nesterenko, M. Akouche, H. El Siblani, J.-M. Goupil, B. Rigaud, D. Minoux, J.-P. Dath, V. Valtchev, Supported Embryonic Zeolites and their Use to Process Bulky Molecules, ACS Catal. 8 (2018) 8199–8212. https://doi.org/10.1021/acscatal.8b01936.
[49] J. Hu, L. Yu, J. Deng, Y. Wang, K. Cheng, C. Ma, Q. Zhang, W. Wen, S. Yu, Y. Pan, J. Yang, H. Ma, F. Qi, Y. Wang, Y. Zheng, M. Chen, R. Huang, S. Zhang, Z. Zhao, J. Mao, X. Meng, Q. Ji, G. Hou, X. Han, X. Bao, Y. Wang, D. Deng, Sulfur vacancy-rich MoS_2 as a

catalyst for the hydrogenation of CO2 to methanol, Nat. Catal. 4 (2021) 242–250. https://doi.org/10.1038/s41929-021-00584-3.
[50] E.D. Garcia, Effect of the support on the activity and morphology of hydrodesulfurization catalysts, phdthesis, Normandie Université, 2017. https://tel.archives-ouvertes.fr/tel-01729093 (accessed August 23, 2022).
[51] S.-H. Lee, M.J. Seong, C.E. Tracy, A. Mascarenhas, J.R. Pitts, S.K. Deb, Raman spectroscopic studies of electrochromic a-MoO_3 thin films, Solid State Ion. 147 (2002) 129–133. https://doi.org/10.1016/S0167-2738(01)01035-9.
[52] S.R. Stojkovic, B. Adnadjevic, Investigation of the NaA zeolite crystallization mechanism by i.r. spectroscopy, Zeolites. 8 (1988) 523–525. https://doi.org/10.1016/S0144-2449(88)80230-6.
[53] P.K. Dutta, D.C. Shieh, M. Puri, Correlation of framework Raman bands of zeolites with structure, Zeolites. 8 (1988) 306–309. https://doi.org/10.1016/S0144-2449(88)80127-1.
[54] A. Martinelli, S. Creci, S. Vavra, P.-A. Carlsson, M. Skoglundh, Local anisotropy in single crystals of zeotypes with the MFI framework structure evidenced by polarised Raman spectroscopy, Phys. Chem. Chem. Phys. 22 (2020) 1640–1654. https://doi.org/10.1039/C9CP06199A.
[55] Y. Yao, K. Ao, P. Lv, Q. Wei, MoS2 Coexisting in 1T and 2H Phases Synthesized by Common Hydrothermal Method for Hydrogen Evolution Reaction, Nanomaterials. 9 (2019). https://doi.org/10.3390/nano9060844.
[56] N.H. Attanayake, A.C. Thenuwara, A. Patra, Y.V. Aulin, T.M. Tran, H. Chakraborty, E. Borguet, M.L. Klein, J.P. Perdew, D.R. Strongin, Effect of Intercalated Metals on the Electrocatalytic Activity of 1T-MoS_2 for the Hydrogen Evolution Reaction, ACS Energy Lett. 3 (2018) 7–13. https://doi.org/10.1021/acsenergylett.7b00865.
[57] X. Li, J. Zhang, R. Wang, H. Huang, C. Xie, Z. Li, J. Li, C. Niu, In Situ Synthesis of Carbon Nanotube Hybrids with Alternate MoC and MoS_2 to Enhance the Electrochemical Activities of MoS_2, Nano Lett. 15 (2015) 5268–5272. https://doi.org/10.1021/acs.nanolett.5b01579.
[58] Z. Zhao, F. Qin, S. Kasiraju, L. Xie, M.K. Alam, S. Chen, D. Wang, Z. Ren, Z. Wang, L.C. Grabow, J. Bao, Vertically Aligned MoS2/Mo2C hybrid Nanosheets Grown on Carbon Paper for Efficient Electrocatalytic Hydrogen Evolution. ACS Catalysis,7 (2017). 7312-7318. https://doi-org.inc.bib.cnrs.fr/10.1021/acscatal.7b02885
[59] J. Jeon, Y. Park, S. Choi, J. Lee, S.S. Lim, B.H. Lee, Y.J. Song, J.H. Cho, Y.H. Jang, S. Lee, Epitaxial Synthesis of Molybdenum Carbide and Formation of a Mo_2C/MoS_2 Hybrid Structure *via* Chemical Conversion of Molybdenum Disulfide, ACS Nano. 12 (2018) 338–346. https://doi.org/10.1021/acsnano.7b06417.
[60] T. Xiao, A.P.E. York, K.S. Coleman, J.B. Claridge, J. Sloan, J. Chanrock, M.L.H. Green, Effect of carburising agent on the structure of molybdenum carbides, J. Mater. Chem. 11 (2001) 3094–3098. https://doi.org/doi-org.inc.bib.cnrs.fr/10.1039/B104011C.
[61] J.-S. Choi, V. Schwartz, E. Santillan-Jimenez, M. Crocker, S. Lewis, M. Lance, H. Meyer, K. More, Structural Evolution of Molybdenum Carbides in Hot Aqueous Environments and Impact on Low-Temperature Hydroprocessing of Acetic Acid, Catalysts. 5 (2015) 406–423. https://doi.org/10.3390/catal5010406.
[62] T. Xiao, A.P.E. York, V.C. Williams, H. Al-Megren, A. Hanif, X. Zhou, M.L.H. Green, Preparation of Molybdenum Carbides Using Butane and Their Catalytic Performance, Chem. Mater. 12 (2000) 3896–3905. https://doi.org/10.1021/cm001157t.
[63] T. Mo, J. Xu, Y. Yang, Y. Li, Effect of carburization protocols on molybdenum carbide synthesis and study on its performance in CO hydrogenation, Catal. Today. 261 (2016) 101–115. https://doi.org/10.1016/j.cattod.2015.07.014.
[64] M. Kakihana, M. Osada, Raman Spectroscopy as a Characterization Tool for Carbon Materials, in: Carbon Alloys, Elsevier, (2003) 285-298. https://doi.org/10.1016/B978-008044163-4/50018-8.

[65] G.P. Froment, B.O. Van de Steene, P.S. Van Damme, S. Narayanan, A.G. Goossens, Thermal Cracking of Ethane and Ethane-Propane Mixtures, Ind. Eng. Chem. Process Des. Dev. 15 (1976) 495–504. https://doi.org/10.1021/i260060a004.
[66] M.S. Shokrollahi Yancheshmeh, S. Seifzadeh Haghighi, M.R. Gholipour, O. Dehghani, M.R. Rahimpour, S. Raeissi, Modeling of ethane pyrolysis process: A study on effects of steam and carbon dioxide on ethylene and hydrogen productions, Chem. Eng. J. 215–216 (2013) 550–560. https://doi.org/10.1016/j.cej.2012.10.078.